J Therm Anal Calorim
DOI 10.1007/s10973-015-4708-8

An advanced reaction model determination methodology in solid-state kinetics based on Arrhenius parameters variation

Part I. Thermal dehydration kinetic analysis of $Cu_4SO_4(OH)_6$

Seyed Hadi Shahcheraghi[1] · Gholam Reza Khayati[2] · Mohammad Ranjbar[1]

Received: 9 February 2015 / Accepted: 12 April 2015

Abstract The variation in the activation energy with the conversion degree of reaction is generally due to the overlapping of parallel or consecutive reactions, and the solution of the problem must imply the deconvolution of the overlapping reaction rather than fitting the experimental curve by assuming variable kinetic parameters. Furthermore, determination of the most probable reaction mechanism model(s) in complicated multi-step reactions kinetics is confronting with the activation energy and the pre-exponential factor variations, as the well-known methods of the thermal analysis are not suitable for determination of the reaction mechanism model(s). To solve this problem, an advanced method for determination of reaction mechanism model based on distributed activation energy model and Arrhenius parameters variation is put forward. This method appears to accurately simulate single-step as well as multi-step reactions kinetics. The proposed method is experimentally verified by taking an experimental example of non-isothermal decomposition kinetics of $Cu_4SO_4(OH)_6$ for the tenorite (CuO) nanoparticles preparation. The results are compared with the iterative procedure and the Arshad and Maaroufi method and effectively interpreted.

Keywords Solid thermal decomposition · Distributed activation energy model · Solid-state kinetics · Multi-step reactions kinetics · Reaction mechanism model · Tenorite nanoparticles

Introduction

In solid-state reactions, appropriate kinetic equations, rate-limiting steps, and calculation of kinetic parameters could supply a deeper conception into the possible mechanisms of transformation [1]. A major limitation of the well-known reaction model determination methods is the use of approximations or an average value for activation energy (apparent activation energy) and pre-exponential factor instead of activation energy and pre-exponential factor variations or distributions. Furthermore, determination of the most probable reaction mechanism model(s) in complicated multi-step reactions kinetics is confronting with the activation energy and the pre-exponential factor variations, as these methods are not suitable for determination of the reaction mechanism model(s).

Arshad and Maaroufi [2] in 2014 proposed a reaction model determination methodology based on variable activation energy concept. They supposed the pre-exponential factor varied with temperature by following the relationship as given below:

$$A = A_0\left(\frac{T}{T_0}\right)^n \tag{1}$$

where A_0 is the value of pre-exponential factor at initial temperature T_0 and n is a numerical constant. Then, after substituting the value of A from Eq. (1) into general kinetics equation of solid-state reactions, its differentiation with respect to degree of conversion and its simplification generated the new equation. However, for simplicity, they supposed the parameter n (in Eq. 1) was of order unity, and

✉ Seyed Hadi Shahcheraghi
sh.shahcheraghi@eng.uk.ac.ir

[1] Department of Mineral Processing Engineering, Shahid Bahonar University of Kerman, Kerman, Iran

[2] Department of Materials Science and Engineering, Shahid Bahonar University of Kerman, Kerman, Iran

Published online: 15 May 2015

the term $[\beta (n + E_\alpha/RT)/T]$ was approximated to $[\beta E_\alpha/RT^2]$ due to high values of activation energy of solid-state reactions, where β is the heating rate, R is the gas constant, and E_α is the apparent activation energy. Generally, the parameter n (in Eq. 1) is not of order unity, necessarily [3]. Also, the activation energies of solid-state reactions essentially are not enough high to compensate this assumption. For example, the activation energy variations for the kinetics of non-isothermal and isothermal curing reaction of DGEBA (diglycidyl ether of bisphenol-A) with a nonlinear star-like aliphatic polyamine curing agent for epoxy resins, *N*,*N*,*N*′,*N*′,*N*″-penta(3-aminopropyl)-diethylenetriamine (PADT), are between 20 and 56 kJ mol^{-1} [4]. Also, the activation energy variations for the kinetics of DGEBA thermosets cured with a hyperbranched poly (ethyleneimine) and an aliphatic triamine are between 40 and 60 kJ mol^{-1} [5].

Hence, even though the methodology describes the kinetics of non-isothermal curing reaction of DGEBA with an aliphatic diamine (to yield epoxy resin) well, it will not probably be comprehensive method for determination of mechanism model(s) of solid-state reactions.

To improve the conceptual principle of reaction kinetics, an advanced method of reaction mechanism model determination based on Arrhenius parameters variation is put forward. This method appears to accurately simulate single-step as well as multi-step reactions kinetics. The proposed method is verified by taking an experimental example of non-isothermal decomposition kinetics of $Cu_4SO_4(OH)_6$. Then, the results are compared with iterative procedure and methodology of Arshad and Maaroufi [2] and effectively interpreted.

To the best of our knowledge, non-isothermal kinetics modeling of CuO nanoparticles preparation from industrial leaching solution has not been investigated yet. Our current contribution will provide the comprehensive data toward a better understanding of the mechanism(s) of $Cu_4SO_4(OH)_6$ dissociation.

Koga et al. [6] in 1997 studied the reaction pathway of the thermal decomposition of synthetic brochantite [$Cu_4SO_4(OH)_6$], which was prepared by the precipitates of basic copper (II) sulfate at 298 K by adding 0.1 M NaOH solution dropwise at the rate of 1.0 mL min^{-1} with stirring to 100 mL of 0.1 M $CuSO_4$ solution until the pH of the resulting solution was equal to 8.0. The results showed that the dehydration process was characterized by dividing into two kinetic processes with a possible formation of an intermediate compound, $Cu_4O(OH)_4SO_4$, which was followed by the crystallization mixture of CuO and $CuO{\cdot}CuSO_4$ at around 776 K. Moreover, the thermal desulferation process was influenced by the gross diffusion of the gaseous product SO_3, which was governed by the advancement of the overall reaction interface from the top surface of the sample particle assemblage to the bottom.

In the present work, we studied only the thermal dehydration kinetics of $Cu_4SO_4(OH)_6$. Also, other stages of thermal decomposition of $Cu_4SO_4(OH)_6$ will be studied in future works.

Materials and methods

Synthesis of precursor from pregnant leach solution (PLS)

Copper leaching, solvent extraction and electrowinning are the main hydrometallurgical processes for oxidized and low-grade copper ore processing. Leaching involves dissolving Cu^{2+} from copper-containing minerals into an aqueous H_2SO_4 solution, known as the lixiviant, to produce a pregnant leach solution (PLS). In addition to copper, the PLS will also contain other impurity species, such as Fe, Al, Co, Mn, Zn, Mg, and Ca, that may be present in the ore and are leached with the copper [7–11]. In the present work, the PLS was obtained from the industrial copper heap-leaching solution of Miduk Copper mine in Iran.

In the present study, the solvent extraction process was used for the purification of PLS. In copper solvent extraction, the aqueous copper leach solution is concentrated and purified using a copper-selective organic solution. The solvent extraction process consists of extraction and stripping processes, both of which may contain parallel and series unit processes. In the extraction stage, the copper is extracted from the leach solution into the organic solution [7–11]. In the Miduk copper mine, 5-nonylsalicylaldoxime is widely used as an organic extractant.

The concentration of solvent extractor in organic phase (5-nonylsalicylaldoxime) was 8 %. The rest of the organic phase was the proprietary diluent (a mixture of kerosene: 36 %, RESOL 8411: 30 %, and RESOL 8401: 26 %). One liter of the organic phase was added to 1 L of leaching solution in a separating funnel. The mixture was shaken thoroughly for 4 min. After separation of the two phases, the aqueous phase was put aside, and solvent extraction was done on the organic phase again.

Then, an equal volume of sulfuric acid solution (200 g L^{-1}) was added to the separating funnel which contained the organic phase. After mixing and separation of two phases, the organic phase was put aside, and the aqueous phase which contained $CuSO_4$ was used for the synthesis of precursor.

The inductive coupled plasma (ICP-MS, Varian 715-ES) analysis of the PLS and aqueous solution after stripping (diluted $CuSO_4$) was reported in Table 1. Accordingly, the impurity species amounts of aqueous solution after stripping are lower than 100 mg L^{-1}, and there was no significant effect on the run of $Cu_4SO_4(OH)_6$ decomposition [12–16].

Table 1 Chemical analysis of the PLS (before solvent extraction) and aqueous phase (after solvent extraction)

Solution type	Elements/mg L^{-1}									
	Cu	Fe	Mn	Pb	Al	Se	Cr	Te	Cd	Sb
Copper pregnant leach solution (PLS)	2960.30	2671.15	87.23	2.00	4430.12	1.20	2.27	4.51	1.35	2.56
Aqueous phase (after stripping)	2558.64	89.12	12.43	<1	91.26	<1	1.08	1.28	<1	<1

Brochantite [$Cu_4SO_4(OH)_6$], as precursor, was prepared by the addition of a 0.5 M Na_2CO_3 solution to a 0.05 M (2.56 g L^{-1}) previous stage $CuSO_4$ solution at a rate of 4 mL min^{-1} (dropwise) for 95 min with vigorous stirring (1500 rpm) at 55 °C. The green precipitate (brochantite) was then filtered and rinsed three times with warm deionized water and dried at 50 °C for several hours.

Methods of sample characterization

To study the kinetics of $Cu_4SO_4(OH)_6$ decomposition, 7 ± 0.5 mg of the precursor is studied through DSC–TG (German NETZSCH-STA409C thermal analyzer) in a dynamic (50 mL min^{-1}) atmosphere of argon at different heating rates of 5, 10, 15, and 20 °C min^{-1} in the temperature range of 25–800 °C. For each sample and heating rate, three repetitive TG curves were obtained to assure reproducibility of the results.

The crystalline structures, morphology, and size of CuO nanoparticles were characterized by XRD (Philips, X'pert-MPD system using Cu K_α) and SEM (Tescan Vega), respectively. The morphology of the synthesized brochantite [$Cu_4SO_4(OH)_6$] was examined by HRSEM (Hitachi S-4160). IR spectra were recorded in the 400–4000 cm^{-1} range with a resolution of 4 cm^{-1}, using Bruker tensor 27 FTIR spectrometer with RT-DIATGS detector and KBr pellet technique.

Nitrogen adsorption/desorption isotherms were measured by ASAP 2020 Micromeritics surface area analyzer. The specific surface areas were assessed according to the standard Brunauer–Emmett–Teller (BET) method. The pore size distributions and total pore volume were determined from adsorption branches of isotherms by the Barrett–Joyner–Halenda (BJH) method.

Theoretical

Theoretical background of solid-state kinetics

Generally, the rate of degradation reaction can be described in terms of two functions, i.e., $k(T)$ and $f(\alpha)$, thus,

$$\frac{d\alpha}{dt} = \beta\frac{d\alpha}{dT} = k(T_\alpha)f(\alpha) \tag{2}$$

where α is the degree of conversion, t is the reaction time, T_α is the absolute temperature, β is the heating rate, $k(T_\alpha)$ is the rate constant, and $f(\alpha)$ is the type of reaction or function of reaction mechanism. In TG analysis, the degree of conversion can be defined as the ratio of actual mass loss to the total mass loss corresponding to the decomposition process [17–20]:

$$\alpha = \frac{m_0 - m}{m_0 - m_f} \tag{3}$$

where m_0, m, and m_f are the initial, actual, and final masses of the sample, respectively. The dependence of the reaction rate constant on temperature can be described by Arrhenius equation [17, 21–23]:

$$k(T) = A_\alpha \exp\left(-\frac{E_\alpha}{RT_\alpha}\right) \tag{4}$$

where A_α is the pre-exponential factor, R is the gas constant (8.314 J mol^{-1} K^{-1}), and E_α is the apparent activation energy. To estimate activation energy, various methods have been proposed. These methods can be generally categorized as: (a) isoconversional and (b) model-fitting methods [21–25]. In addition, there are more complex "model-free" methods, such as the nonlinear isoconversional method by Vyazovkin and Wight [26] and Vyazovkin [27], solutions of which can only be obtained using computer algorithms.

Due to great calculation accuracy and versatile applicability for various heating programs [21–23, 28], the advanced isoconversional methods developed by Vyazovkin, the Vyazovkin method, was adopted to analyze the non-isothermal reaction. Specifically, the Vyazovkin method is applicable to a non-isothermal kinetic process with a series of linear heating, which can be written as [17, 21–23]:

$$\Phi(E_\alpha) = \sum_{i=1}^{n}\sum_{j\neq 1}^{n}\frac{I(E_\alpha, T_{\alpha,i})\beta_j}{I(E_\alpha T_{\alpha,j})\beta_i} \tag{5}$$

$$I\left(E_\alpha, T_{\alpha,i}\right) = \int_{T_{\alpha-\Delta\alpha}}^{T_\alpha} \exp\left(-\frac{E_\alpha}{RT_\alpha}\right)dT \tag{6}$$

where β_i and β_j represent the different heating rates, T_α and $T_{\alpha-\Delta\alpha}$ are the reaction temperatures corresponding to α and $\Delta\alpha$, respectively. Minimizing Eq. (5) for each α with a certain conversion increment (usually $\Delta\alpha = 0.05$) results in the correction of E_α with α. The detailed descriptions of how to use the Vyazovkin method to treat calorimetric data can be acquired elsewhere [17, 21–23, 29, 30].

Arshad and Maaroufi method

Arshad and Maaroufi [2] in 2014 proposed a reaction model determination methodology based on variable activation energy concept. They supposed the pre-exponential factor varied with temperature by Eq. (1). Then, after substituting the value of A from Eq. (1) into Eq. (2), its differentiation with respect to degree of conversion and its simplification (for simplicity, they supposed $n = 1$ (in Eq. 1) and the term $[\beta\,(n + E_\alpha/RT)/T] \approx [\beta E_\alpha/RT^2]$ due to high values of activation energy of solid-state reactions) generated the following equation [2]:

$$h(\alpha) = \frac{f'(\alpha)}{f(\alpha)} = \left(\frac{1}{\frac{\mathrm{d}\alpha}{\mathrm{d}t}}\right)\left[\frac{\left(\frac{\mathrm{d}^2\alpha}{\mathrm{d}t^2}\right)}{\left(\frac{\mathrm{d}\alpha}{\mathrm{d}t}\right)} + \frac{\beta}{RT}\frac{\mathrm{d}E_\alpha}{\mathrm{d}T} - \frac{\beta E_\alpha}{RT^2}\right] \tag{7}$$

where $h(\alpha)$ is an expression to describe the ratio between differentiated and actual reaction model.

The iterative procedure

The iterative procedure [31–35] is widely used to estimate the most correct reaction mechanism, i.e., $g(\alpha)$ function,

$$\ln(g(\alpha)) = \left[\ln\left(\frac{A_\alpha E_\alpha}{R}\right) + \ln\left(\frac{\exp(-u_\alpha)}{u_\alpha^2}\right) + \ln(h(u_\alpha))\right] - \ln(\beta) \tag{8}$$

where $u_\alpha = E_\alpha/RT_\alpha$, and $h(u_\alpha)$ is expressed by the fourth Senum and Yang approximation formulas [21–23]. The degrees of conversion α corresponding to multiple rates at the same temperature are in the left side of Eq. (8); combined with well-known mechanism functions (Table 2), the slope of the straight line and the linear correlation coefficient (r) is obtained from the plot of $\ln(g(\alpha))$ versus $\ln(\beta)$. The most probable mechanism function is the one for which the value of the slope is near 1, and the correlation coefficient is higher.

If several $g(\alpha)$ functions follow this requirement, the degrees of conversion corresponding to multiple heating rates at several temperatures are used to calculate the most probable mechanism by the same method. The function, whose slope value is the closest to 1 and the correlation coefficient that is also high at all these temperatures, is considered to be the most probable mechanism function. In this work, the proposed method results are compared with iterative procedure and the Arshad and Maaroufi method.

Distributed activation energy model (DAEM)

The DAEM is a powerful method that has been used very successfully in the kinetic analysis of complex materials [36–38]. The model assumes that many irreversible first-order parallel reactions that have different rate parameters and a Gaussian distribution of activation energies occur simultaneously. The DAEM can be described by Eq. (9) [36–38]:

$$1 - \alpha = \int_0^\infty \exp\left(-\int_0^T \frac{A_\alpha}{\beta}\exp\left(-\frac{E_\alpha}{RT_\alpha}\right)\mathrm{d}T\right) f(E_\alpha)\mathrm{d}E_\alpha \tag{9}$$

where $f(E_\alpha)$ is the distribution curve of the activation energy to represent the differences in the activation energies of many first-order irreversible reactions. A new method was presented by Miura [36] for estimating $f(E_\alpha)$ and A_α in the DAEM. He does not assume a predefined activation energy distribution and supposes a non-constant frequency factor [28]. In supposed method, $f(E_\alpha)$ and A_α can be estimated accurately. The equation is expressed as follows [36]:

$$\ln\left(\frac{\beta}{T_\alpha^2}\right) = \ln\left(\frac{A_\alpha R}{E_\alpha}\right) + 0.6075 - \frac{E_\alpha}{RT_\alpha} \tag{10}$$

The proposed method for determination of reaction mechanism

Non-isothermal kinetics

Generally, in the thermal analysis, degree of conversion, energy of activation, and pre-exponential factor vary in the following way:

$$\alpha = \omega_1(T,t) \quad E = \omega_2(\alpha) = E_\alpha \quad A = \omega_3(\alpha) = A_\alpha$$

The overall change in the reaction rate as reaction advances can be described by differentiating Eq. (2) with respect to the degree of conversion as:

$$\frac{\mathrm{d}}{\mathrm{d}\alpha}\left(\frac{\mathrm{d}\alpha}{\mathrm{d}t}\right) = \frac{\mathrm{d}\alpha}{\mathrm{d}t}\left[\frac{1}{A_\alpha}\frac{\mathrm{d}A_\alpha}{\mathrm{d}\alpha} - \frac{1}{RT_\alpha}\frac{\mathrm{d}E_\alpha}{\mathrm{d}\alpha} + \frac{E_\alpha}{RT_\alpha^2}\frac{\mathrm{d}T_\alpha}{\mathrm{d}\alpha} + \frac{f'(\alpha)}{f(\alpha)}\right] \tag{11}$$

Using chain rule of differentiation, $\mathrm{d}/\mathrm{d}\alpha(\mathrm{d}\alpha/\mathrm{d}t) = \mathrm{d}/\mathrm{d}t(\mathrm{d}\alpha/\mathrm{d}t)(\mathrm{d}t/\mathrm{d}\alpha) = (\mathrm{d}^2\alpha/\mathrm{d}t^2)/(\mathrm{d}\alpha/\mathrm{d}t)$, and rearranging Eq. (11) give:

$$\frac{\left(\frac{\mathrm{d}^2\alpha}{\mathrm{d}t^2}\right)}{\left(\frac{\mathrm{d}\alpha}{\mathrm{d}t}\right)^2} = \left[\frac{1}{A_\alpha}\frac{\mathrm{d}A_\alpha}{\mathrm{d}\alpha} - \frac{1}{RT_\alpha}\frac{\mathrm{d}E_\alpha}{\mathrm{d}\alpha} + \frac{E_\alpha}{RT_\alpha^2}\frac{\mathrm{d}T_\alpha}{\mathrm{d}\alpha} + \frac{f'(\alpha)}{f(\alpha)}\right] \tag{12}$$

On the basis of Eq. (10), the pre-exponential factor can be written as:

$$A_\alpha = \frac{E_\alpha\beta}{RCT_\alpha^2}\exp\left(\frac{E_\alpha}{RT_\alpha}\right) \tag{13}$$

where C is a numerical constant. Substituting the value of A_α from Eq. (13) into Eq. (12) yields the following equation:

Table 2 Mathematical expressions of functions $g(\alpha)$ and $f(\alpha)$ with their physical meanings

No.	Model	$g(\alpha)$	$f(\alpha)$	Rate-determining mechanism
1. Chemical process or mechanism non-invoking equations	$F_{1/3}$	$1-(1-\alpha)^{2/3}$	$(3/2)(1-\alpha)^{1/3}$	Chemical reaction
	$F_{3/4}$	$1-(1-\alpha)^{1/4}$	$(4)(1-\alpha)^{3/4}$	Chemical reaction
	$F_{3/2}$	$(1-\alpha)^{-1/2}-1$	$(2)(1-\alpha)^{3/2}$	Chemical reaction
	F_2	$(1-\alpha)^{-1}-1$	$(1-\alpha)^2$	Chemical reaction
	F_3	$(1-\alpha)^{-2}-1$	$(1/2)(1-\alpha)^3$	Chemical reaction
2. Acceleratory rate equations	$P_{3/2}$	$\alpha^{3/2}$	$(2/3)\alpha^{-1/2}$	Nucleation
	$P_{1/2}$	$\alpha^{1/2}$	$2\alpha^{1/2}$	Nucleation
	$P_{1/3}$	$\alpha^{1/3}$	$3\alpha^{2/3}$	Nucleation
	$P_{1/4}$	$\alpha^{1/4}$	$4\alpha^{3/4}$	Nucleation
	E_1	$\ln(\alpha)$	α	Nucleation
3. Sigmoidal rate equations or random nucleation and subsequent growth	A_1, F_1	$-\ln(1-\alpha)$	$(1-\alpha)$	Assumed random nucleation and its subsequent growth, $n=1$
	$A_{3/2}$	$[-\ln(1-\alpha)]^{2/3}$	$(3/2)(1-\alpha)[-\ln(1-\alpha)]^{1/3}$	Assumed random nucleation and its subsequent growth, $n=1.5$
	A_2	$[-\ln(1-\alpha)]^{1/2}$	$(2)(1-\alpha)[-\ln(1-\alpha)]^{1/2}$	Assumed random nucleation and its subsequent growth, $n=2$
	A_3	$[-\ln(1-\alpha)]^{1/3}$	$(3)(1-\alpha)[-\ln(1-\alpha)]^{2/3}$	Assumed random nucleation and its subsequent growth, $n=3$
	A_4	$[-\ln(1-\alpha)]^{1/4}$	$(4)(1-\alpha)[-\ln(1-\alpha)]^{3/4}$	Assumed random nucleation and its subsequent growth, $n=4$
	A_u	$\ln[\alpha/(1-\alpha)]$	$\alpha\,(1-\alpha)$	Branching nuclei
4. Deceleratory rate equations (phase boundary reaction)	R_1, F_0, P_1	α	1	Contracting disk
	R_2, $F_{1/2}$	$1-(1-\alpha)^{1/2}$	$(2)(1-\alpha)^{1/2}$	Contracting cylinder
	R_3, $F_{2/3}$	$1-(1-\alpha)^{1/3}$	$(3)(1-\alpha)^{2/3}$	Contracting sphere
5. Deceleratory rate equations (based on the diffusion mechanism)	D_1	α^2	$1/(2\alpha)$	One-dimensional diffusion
	D_2	$\alpha+[(1-\alpha)\ln(1-\alpha)]$	$[-\ln(1-\alpha)]^{-1}$	Two-dimensional diffusion
	D_3	$[1-(1-\alpha)^{1/3}]^2$	$(3/2)(1-\alpha)^{2/3}[1-(1-\alpha)^{1/3}]^{-1}$	Three-dimensional diffusion, spherical symmetry
	D_4	$1-(2\alpha/3)-(1-\alpha)^{2/3}$	$(3/2)[(1-\alpha)^{-1/3}-1]^{-1}$	Three-dimensional diffusion, cylindrical symmetry
	D_5	$[(1-\alpha)^{-1/3}-1]^2$	$(3/2)(1-\alpha)^{4/3}[(1-\alpha)^{-1/3}-1]^{-1}$	Three-dimensional diffusion
	D_6	$[(1+\alpha)^{1/3}-1]^2$	$(3/2)(1+\alpha)^{2/3}[(1+\alpha)^{1/3}-1]^{-1}$	Three-dimensional diffusion
	D_7	$1+(2\alpha/3)-(1+\alpha)^{2/3}$	$(3/2)[(1+\alpha)^{-1/3}-1]^{-1}$	Three-dimensional diffusion
	D_8	$[(1+\alpha)^{-1/3}-1]^2$	$(3/2)(1+\alpha)^{4/3}[(1+\alpha)^{-1/3}-1]^{-1}$	Three-dimensional diffusion
6. Other kinetics equations with unjustified mechanism	G_1	$1-(1-\alpha)^2$	$1/[(2)(1-\alpha)]$	
	G_2	$1-(1-\alpha)^3$	$1/[(3)(1-\alpha)^2]$	
	G_3	$1-(1-\alpha)^4$	$1/[(4)(1-\alpha)^3]$	
	G_4	$[-\ln(1-\alpha)]^2$	$(1/2)(1-\alpha)[-\ln(1-\alpha)]^{-1}$	
	G_5	$[-\ln(1-\alpha)]^3$	$(1/3)(1-\alpha)[-\ln(1-\alpha)]^{-2}$	
	G_6	$[-\ln(1-\alpha)]^4$	$(1/4)(1-\alpha)[-\ln(1-\alpha)]^{-3}$	
	G_7	$[1-(1-\alpha)^{1/2}]^{1/2}$	$(4)[(1-\alpha)[1-(1-\alpha)]^{1/2}]^{1/2}$	
	G_8	$[1-(1-\alpha)^{1/3}]^{1/2}$	$(6)(1-\alpha)^{2/3}[1-(1-\alpha)^{1/3}]^{1/2}$	

$$\frac{\left(\frac{\mathrm{d}^2\alpha}{\mathrm{d}t^2}\right)}{\left(\frac{\mathrm{d}\alpha}{\mathrm{d}t}\right)^2}=\left[\frac{1}{E_\alpha}\frac{\mathrm{d}E_\alpha}{\mathrm{d}\alpha}-\frac{2}{T_\alpha}\left(\frac{\mathrm{d}T_\alpha}{\mathrm{d}\alpha}\right)+\frac{f'(\alpha)}{f(\alpha)}\right] \tag{14}$$

Employing chain rule of differentiation, $\mathrm{d}E_\alpha/\mathrm{d}\alpha=(\mathrm{d}E/\mathrm{d}T)(\mathrm{d}T/\mathrm{d}\alpha)=\beta(\mathrm{d}E/\mathrm{d}T)/(\mathrm{d}\alpha/\mathrm{d}t)$ and also $\mathrm{d}T_\alpha/\mathrm{d}\alpha=1/(\mathrm{d}\alpha/\mathrm{d}T)=\beta/(\mathrm{d}\alpha/\mathrm{d}t)$, and substituting them into Eq. (14) yield the following equation:

$$\frac{\left(\frac{d^2\alpha}{dt^2}\right)}{\left(\frac{d\alpha}{dt}\right)^2} = \left[\frac{\beta}{E_\alpha}\frac{dE_\alpha}{dT}\left(\frac{1}{\frac{d\alpha}{dt}}\right) - \frac{2\beta}{T_\alpha}\left(\frac{1}{\frac{d\alpha}{dt}}\right) + \frac{f'(\alpha)}{f(\alpha)}\right] \quad (15)$$

Rearrangement of Eq. (15) gives:

$$\frac{f'(\alpha)}{f(\alpha)} = \mathrm{Sh}(\alpha) = \left(\frac{1}{\frac{d\alpha}{dt}}\right)\left[\frac{\left(\frac{d^2\alpha}{dt^2}\right)}{\left(\frac{d\alpha}{dt}\right)} - \frac{\beta}{E_\alpha}\frac{dE_\alpha}{dT} + \frac{2\beta}{T_\alpha}\right] \quad (16)$$

where Sh(α) is the ratio between differentiated and actual reaction model. It is clear from this equation that its right-hand side can be obtained by experimental thermoanalytical data, while left-hand side can be simulated for the reaction models. A fair fitting between curves generated from thermoanalytical data and theoretical models can result in the appropriate reaction models. Equation (16) takes the following form when the reaction follows single-step kinetics and $dE_\alpha/dT \approx 0$:

$$\frac{f'(\alpha)}{f(\alpha)} = \mathrm{Sh}(\alpha) = \left(\frac{1}{\frac{d\alpha}{dt}}\right)\left[\frac{\left(\frac{d^2\alpha}{dt^2}\right)}{\left(\frac{d\alpha}{dt}\right)} + \frac{2\beta}{T_\alpha}\right] \quad (17)$$

Moreover, if the difference between the maximum and minimum values of E_α was less than 20–30 % of the average E_α, the activation energy was independent from α [28, 39]. In this state, because of $dE_\alpha/dT \neq 0$, Eq. (16) was used for determination of reaction mechanism model.

Furthermore, the reaction model(s) for multi-step processes could be determined using integration of Sh(α):

$$\int_0^1 \mathrm{Sh}(\alpha)d\alpha = \int_0^1 \frac{f'(\alpha)}{f(\alpha)}d\alpha = f(\alpha) \quad (18)$$

Isothermal kinetics

Sh(α) in isothermal kinetics can be determined by putting $\beta = (dT/dt) = 0$ in Eq. (16) and rearranging it as following:

$$\frac{f'(\alpha)}{f(\alpha)} = \mathrm{Sh}(\alpha) = \frac{\left(\frac{d^2\alpha}{dt^2}\right)}{\left(\frac{d\alpha}{dt}\right)^2} - \frac{1}{E_\alpha}\frac{dE_\alpha}{d\alpha} \quad (19)$$

In isothermal kinetics, the evaluation of reaction model follows the similar route as discussed in the previous section. If the reaction consists of only one step ($dE/d\alpha \approx 0$), Eq. (19) can be written as following equation:

$$\frac{f'(\alpha)}{f(\alpha)} = \mathrm{Sh}(\alpha) = \frac{\left(\frac{d^2\alpha}{dt^2}\right)}{\left(\frac{d\alpha}{dt}\right)^2} \quad (20)$$

It should be mentioned, if reaction follows single-step isothermal kinetics then its mechanistic information can be directly obtained by thermoanalytical data, independent of its activation energy and pre-exponential factor. Table 3 represents the Sh(α) expression for well-known reaction models.

Results and discussion

Preparation of CuO nanoparticles

Figure 1a shows the XRD pattern of $Cu_4SO_4(OH)_6$ precursor. As shown, almost all diffraction peaks were consistent with monoclinic $Cu_4SO_4(OH)_6$ (JCPDS card No. 01-087-0454). Figure 1b shows typical XRD pattern of CuO nanocrystals prepared at the heating rate of 10 °C min^{-1}. As shown, all the diffraction peaks of nanoparticles (i.e., 32.51, 35.56, 38.74, 46.31, 48.75, 53.51, 58.31, 61.53, 66.24, and 68.13) are consistent with the standard structure (JCPDS card no. 05-0661). Accordingly, the precursor was completely decomposed at about 700 °C into single phase of the pure crystalline CuO. It is well known that crystallite size can be estimated from diffraction pattern analysis by measuring the full width at half maximum (FWHM) measurement and applying the Scherrer equation [40]:

$$D = \frac{\mu\lambda}{\beta\mathrm{Cos}(\theta_0)} \quad (21)$$

where β is the FWHM, μ is the Scherrer constant ($\mu = 0.9$) [12–16, 40, 41], λ is the wavelength in nanometers (the wavelength of Cu K_α is 0.154 nm [12, 13, 41]), θ_0 is the Bragg angle, and D the mean crystallite size (nm) [40]. The peak broadening also depends on the lattice strain induced by mechanical stresses, so that the Williamson–Hall method can be used to improve the analysis [42]. The mean crystallite size of tenorite was calculated to be about 45 nm using Scherrer equation.

Figure 2a, b shows the FT-IR spectra of the $Cu_4SO_4(OH)_6$ precursor and the CuO nanoparticles prepared at the heating rate of 10 °C min^{-1}. The absorption bands (Fig. 2a) around 426, 487, 511, 601, 735, 780, 875, 943, 988, 1088, 1126, 1431, 3275, and 3391 cm^{-1} are attributed to $Cu_4SO_4(OH)_6$ [43, 44]. In Fig. 2b, the peak around 480–585 cm^{-1} is assigned to Cu–O of CuO, confirming the formation of the pure CuO nanoparticles [45–47]. And, the peak at 2363 cm^{-1} corresponds to the atmospheric CO_2 [48].

Figure 3a shows the typical SEM image of CuO nanoparticles prepared at the heating rate of 10 °C min^{-1}. Accordingly, CuO particles exhibit a strong tendency to form nanoparticle agglomerates. Moreover, in the Scherrer method, the average crystallite size of CuO (i.e., 45 nm) was calculated and is not necessarily equal to the particle

Table 3 Mathematical expressions of functions Sh(α) for the well-known reaction functions

No.	Model	$f(\alpha)$	Sh(α)
1. Chemical process or mechanism non-invoking equations	F_n ($n \neq 0,1/2,2/3,1$)	$(1-\alpha)^n/\lvert 1-n\rvert$	$-n/(1-\alpha)$
2. Acceleratory rate equations	P_n ($n \neq 1$)	$(1/n)\alpha^{(1-n)}$	$(1-n)/\alpha$
	E_1	α	$1/\alpha$
3. Sigmoidal rate equations or random nucleation and subsequent growth	A_n	$n(1-\alpha)[-\ln(1-\alpha)]^{(1-1/n)}$	$[1-(1/n)+\ln(1-\alpha)]/[(\alpha-1)\ln(1-\alpha)]$
	F_1	$(1-\alpha)$	$1/(\alpha-1)$
4. Deceleratory rate equations (phase boundary reaction)	R_1, F_0, P_1	1	0
	R_n ($n = 2,3$)	$(n)(1-\alpha)^{1-1/n}$	$(1-n)/[n(1-\alpha)]$
	F_n ($n = 1/2,2/3$)	$(1-\alpha)^n/\lvert 1-n\rvert$	$-n/(1-\alpha)$
5. Deceleratory rate equations (based on the diffusion mechanism)	D_1	$1/(2\alpha)$	$-1/\alpha$
	D_2	$[-\ln(1-\alpha)]^{-1}$	$[1/(1-\alpha)]/\ln(1-\alpha)$
	D_3	$(3/2)(1-\alpha)^{2/3}[1-(1-\alpha)^{1/3}]^{-1}$	$-(2/3)(1-\alpha)^{-1}[1+[(1/2)(1-\alpha)^{1/3}(1-(1-\alpha)^{1/3})^{-1}]]$
	D_4	$(3/2)[(1-\alpha)^{-1/3}-1]^{-1}$	$(1/3)(1-\alpha)^{-4/3}[(1-\alpha)^{-1/3}-1]^{-1}$
	D_5	$(3/2)(1-\alpha)^{4/3}[(1-\alpha)^{-1/3}-1]^{-1}$	$-(4/3)(1-\alpha)^{-1}[1+[(1/4)(1-\alpha)^{-1/3}((1-\alpha)^{-1/3}-1)^{-1}]]$
	D_6	$(3/2)(1+\alpha)^{2/3}[(1+\alpha)^{1/3}-1]^{-1}$	$(2/3)(1+\alpha)^{-1}[1-[(1/2)(1+\alpha)^{1/3}(1-(1+\alpha)^{1/3})^{-1}]]$
	D_7	$(3/2)[(1+\alpha)^{-1/3}-1]^{-1}$	$-(1/3)(1+\alpha)^{-4/3}[(1+\alpha)^{-1/3}-1]^{-1}$
	D_8	$(3/2)(1+\alpha)^{4/3}[(1+\alpha)^{-1/3}-1]^{-1}$	$(4/3)(1+\alpha)^{-1}[1+[(1/4)(1+\alpha)^{-1/3}((1+\alpha)^{-1/3}-1)^{-1}]]$
6. Sestak–Berggren (autocatalytic model)	SB(m,n)	$\alpha^m(1-\alpha)^n$	$(m/\alpha)-(n/(1-\alpha))$

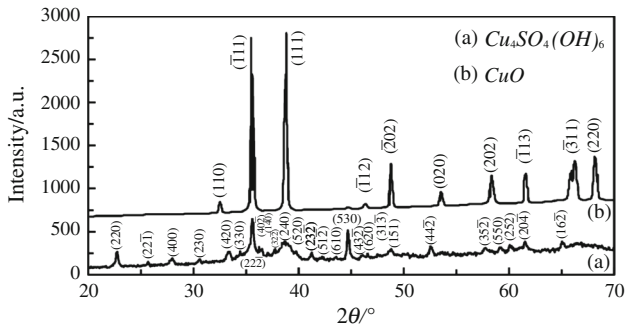

Fig. 1 *a* XRD pattern of the precursor $Cu_4SO_4(OH)_6$ and *b* XRD pattern of CuO nanoparticles prepared at the heating rate of 10 °C min^{-1}

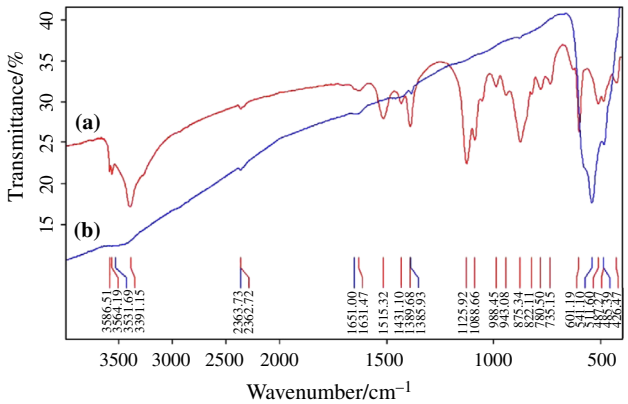

Fig. 2 *a* FT-infrared spectrum of the precursor $Cu_4SO_4(OH)_6$ and *b* FT-infrared spectra of the CuO nanoparticles

size of CuO (Fig. 3a). According to the literature, these differences can be related to the agglomeration and sintering of particles during the heating process [49–52]. The solid-state reconstruction of nanoparticles into aggregates is a usual phenomenon showing a tendency of nanoparticulate systems to restrain unsaturated surface forces via surface recombination [53–55]. EDX analysis of CuO nanoparticles (Fig. 3b) confirms the high purity of the products.

Non-isothermal decomposition of the CuO nanoparticle precursor

The DSC–TG curves of non-isothermal degradation of the CuO nanoparticle precursor at four different heating rates (5, 10, 15, and 20 °C min^{-1}) are shown in Fig. 4. Accordingly, mass losses within three broad steps (about 7, 9, and 12 mass%) were found between 61 and 717 °C. Furthermore, the overall mass loss during decomposition of

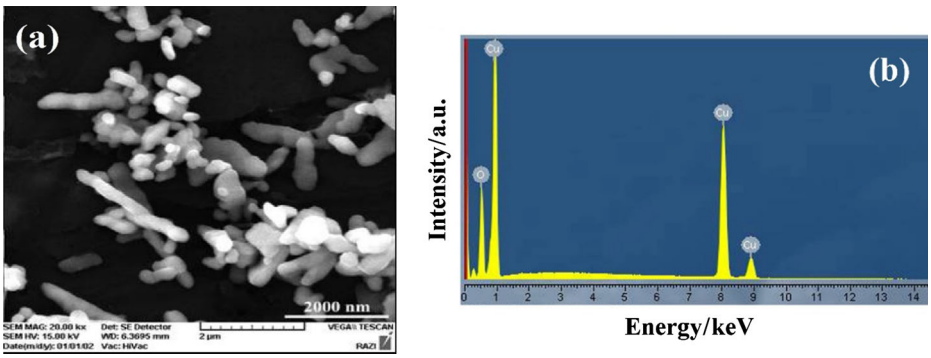

Fig. 3 **a** Typical SEM image of CuO nanoparticles prepared at the heating rate of 10 °C min^{-1} at ×20,000 magnification, **b** EDS patterns of CuO nanoparticles

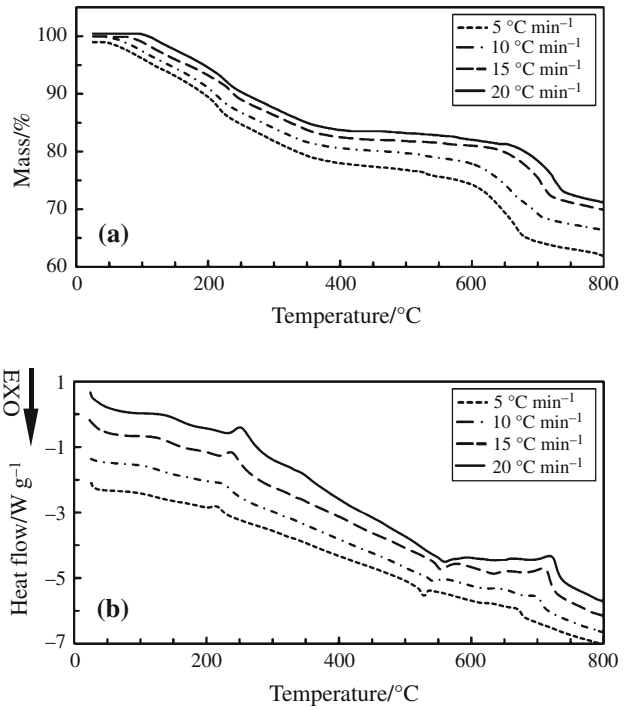

Fig. 4 **a** TG and **b** DSC curves for thermal decomposition of precursor $Cu_4SO_4(OH)_6$ at the heating rates of 5, 10, 15, and 20 °C min^{-1} in argon

$Cu_4SO_4(OH)_6$ to CuO as well as stages I and II of dehydration was calculated on the basis of stoichiometric chemical equations, and similar mass reduction was observed. The first and second one which are between 61 and 250 °C are related to the thermal dehydration that proceeded through the following two processes, respectively [6]:

$$Cu_4SO_4(OH)_6 \rightarrow Cu_4SO_4O(OH)_4 + H_2O \quad (22)$$

$$Cu_4SO_4O(OH)_4 \rightarrow Cu_4SO_4O_3 + 2H_2O \quad (23)$$

The third one which is between 622 and 717 °C is related to the desulferation process. DSC of the precursor (Fig. 4) shows three endothermic peaks around 102 °C (dehydration I), 223 °C (dehydration II), and 700 °C (desulferation) and one exothermic peak, at 541 °C. The exothermic peak between 500 and 600 °C may be due to the crystallization of the amorphous dehydrated product ($Cu_4SO_4O_3$) to CuO and $CuO{\cdot}CuSO_4$ [6].

The same results were obtained in TG analysis, which shows no loss in mass between 533 and 556 °C. Hence, it can be concluded that the endothermic peak at 700 °C is due to the decomposition of the copper oxide sulfate [$CuO{\cdot}CuSO_4$] to CuO [6, 56]. Moreover, by increasing the heating rate, the TG curve and peak of DSC curve shift to a higher temperature, and the final mass loss presents a decreasing trend.

From Fig. 4, by increasing the heating rate, the reaction area was shifted to a higher temperature range. Moreover, onset reaction temperatures, peak temperatures, and end temperatures enhanced with increasing heating rate (Table 4). In the present study, the thermal dehydration kinetics of $Cu_4SO_4(OH)_6$ was studied. Furthermore, other stages of thermal decomposition of $Cu_4SO_4(OH)_6$ will be studied in future work.

The conversional curves (α–T) for thermal dehydrations (I and II) of $Cu_4SO_4(OH)_6$ are indicated in Fig. 5. These conversional curves exhibit the sigmoidal profile, and by increasing heating rate, the curves shift toward the higher temperature. In other words, the higher the heating rate, the higher the temperature for the reaction to reach the identical α.

Calculation of activation energy (E_α)

The dependence of E_α on α for thermal dehydrations (I and II) of $Cu_4SO_4(OH)_6$ is presented in Fig. 6. According to the literature [57–61], if E_α values were independent of α, the decomposition process was dominated by a single reaction step. Therefore, from Fig. 6, it was obvious that thermal dehydration I and dehydration II are a single-step process, but $dE/dT \neq 0$. Based on the Vyazovkin method, E_α showed an almost stable behavior with the average of $E_\alpha = 32.3 \pm 2.1$ and 63.9 ± 1.1 kJ mol^{-1} for thermal dehydration I and dehydration II, respectively, which are more lower than values of the literature (Koga et al. [6],

Table 4 Typical parameters of the thermal dehydration of precursor $Cu_4SO_4(OH)_6$

Reaction	Heating rate/ °C min^{-1}	T_{onset}/°C	T_{peak}/°C	T_{end}/°C
Dehydration I	5	49	97	133
	10	61	102	142
	15	75	119	166
	20	94	130	174
Dehydration II	5	197	214	241
	10	201	223	249
	15	212	237	274
	20	228	251	286

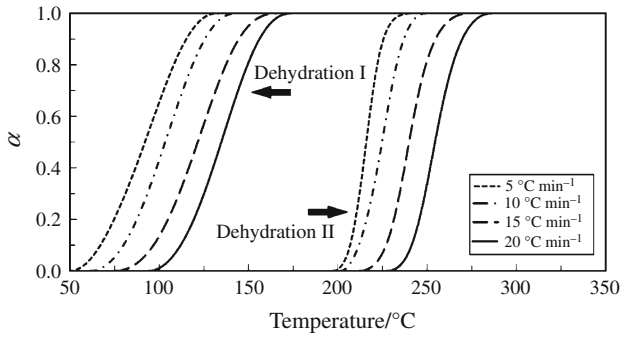

Fig. 5 α–T curves for the thermal dehydrations I and II of precursor $Cu_4SO_4(OH)_6$ at the heating rates of 5, 10, 15, and 20 °C min^{-1} in argon, where α is the degree of conversion and can be well calculated by Eq. (3)

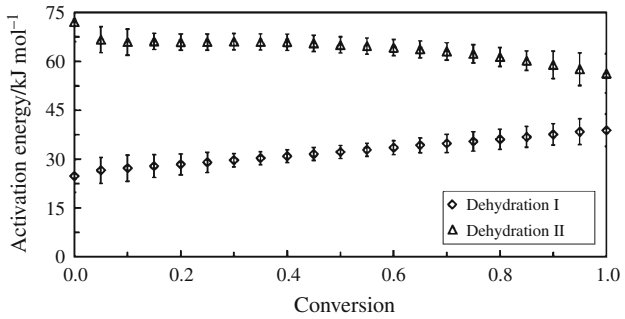

Fig. 6 Dependence of activation energy (E_α) on conversion (α) for the thermal dehydrations I and II of precursor $Cu_4SO_4(OH)_6$

i.e., 158.0 ± 1.3 and 193.1 ± 0.9 kJ mol^{-1} for thermal dehydration I and dehydration II, respectively). It could be related to the nanostructure of the synthetic brochantite [$Cu_4SO_4(OH)_6$] in the present study.

The suitable kinetics models for describing thermal dehydrations (I and II) of $Cu_4SO_4(OH)_6$ were determined using the proposed method, and obtained results were compared with the iterative procedure.

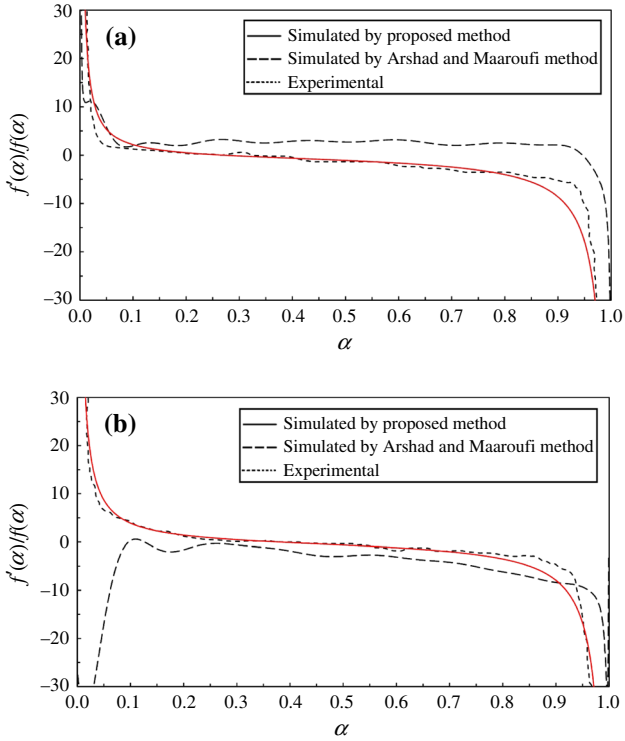

Fig. 7 Agreement between the experimentally obtained Sh(α) curve and proposed method obtained Sh(α) curve and comparison of results with Arshad and Maaroufi method ($\beta = 10$ °C min^{-1}) for **a** the thermal dehydration I and **b** dehydration II of precursor $Cu_4SO_4(OH)_6$; Sh(α) values follow Eq. (16)

Determination of the most probable reaction mechanism function

The proposed method

To verify the validity of the proposed method, thermal decomposition kinetics of $Cu_4SO_4(OH)_6$ were considered, and obtained results were compared with the iterative procedure and the Arshad and Maaroufi method. From Fig. 6, for thermal dehydrations (I and II) of $Cu_4SO_4(OH)_6$, $dE/dT \neq 0$. Hence, the evaluation of the most probable reaction mechanism function using the proposed method follows Eq. (16).

The Sh(α) curves for the thermoanalytical data of the thermal dehydrations (I and II) of $Cu_4SO_4(OH)_6$ at $\beta = 10$ °C min^{-1} are presented in Fig. 7a, b, respectively. As shown, the Sh(α) curves form follows the Avrami–Erofeev A_m-type equation, $m(1-\alpha)[-\ln(1-\alpha)]^{(1-1/m)}$, i.e., $m = 1.453$ (which belongs to diffusion controlled [62]) and $m = 1.908$ (which belongs to interface controlled [62]), for thermal dehydrations I and II, respectively. The reaction model parameters (proposed method) are given in Table 5. Accordingly, as shown in Fig. 7a, b, there was a good agreement between the experimentally obtained

Table 5 Comparison of the kinetic triplets for the thermal dehydration of precursor $Cu_4SO_4(OH)_6$, obtained by the proposed method (Eq. 16) and the iterative procedure (Eq. 8)

Reaction	Iterative procedure			Proposed method		
	E_α/kJ mol^{-1}	A_α/min^{-1}	m	E_α/kJ mol^{-1}	A_α/min^{-1}	m
Dehydration I	32.3	7.5E+03	2	32.3	9.8E+03	1.453
Dehydration II	63.9	1.7E+06	3	63.9	2.5E+06	1.908

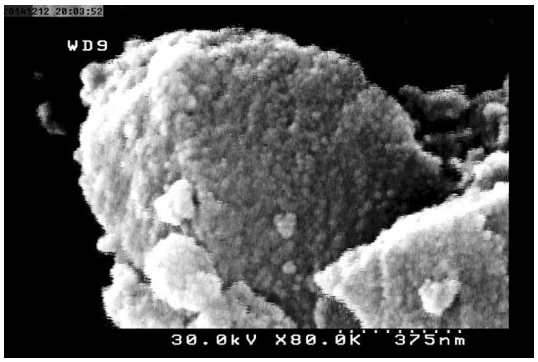

Fig. 8 HRSEM image of the as-received $Cu_4SO_4(OH)_6$ precursor at ×80,000 magnification

Sh(α) curves and A_m model obtained Sh(α) curves ($\beta = 10$ °C min^{-1}).

Moreover, these results were proved by the HRSEM (Fig. 8) and BET (Fig. 9). As shown in Fig. 8, the brochantite [$Cu_4SO_4(OH)_6$] nanoparticles have strong tendency to agglomeration. Therefore, according to Eq. (22), for the thermal dehydration I, some of the OH molecules are aspirated from agglomerated precursor with the mechanism of diffusion controlled, and the porous precursor is made. Then, according to Eq. (23), for the thermal dehydration II, the residual OH molecules are aspirated from porous precursor with the mechanism of interface controlled, and the amorphous precursor is made in view of XRD.

Also, the strong agglomerated structure of precursor and the porous sample structure of the thermal dehydration I were investigated by BET analysis. The data in Fig. 9 display the N_2 adsorption–desorption isotherms confirmed the strong agglomeration of precursor and the porous sample of the thermal dehydration I.

According to the classification given by Brunauer et al. [63, 64], the isotherms determined on both samples are similar to type IV isotherms which are obtained for porous materials ($1.5\ \text{nm} < r_p < 100\ \text{nm}$). According to the IUPAC classification [65], the isotherm determined on the as-received precursor exhibits the type H1 hysteresis loop (Fig. 9a). The type H1 hysteresis loop is attributed to the formation of spherical shape pores with a narrow pores distribution [65, 66]. The BET analysis showed that the as-received precursor structure is the characteristic of bimodal-typed pore size distribution in the range of 2–25 nm

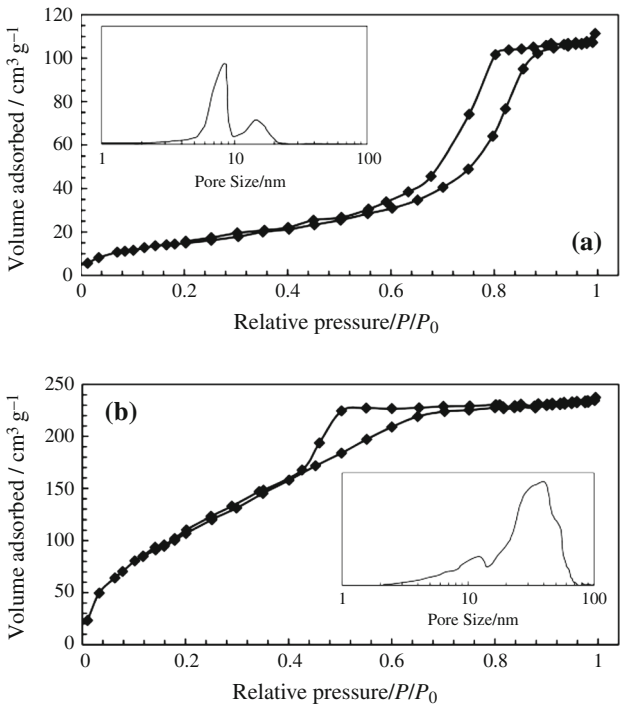

Fig. 9 Nitrogen adsorption–desorption isotherms determined on samples of **a** the as-received precursor and **b** the thermal dehydration I of $Cu_4SO_4(OH)_6$; the *insets* are the pore size distribution

(below 100 nm), which is due to the strong agglomeration of the precursor nanoparticles (the inset in Fig. 9a).

Also, the isotherm determined on the porous sample of the thermal dehydration I exhibits the type H2 hysteresis loop (Fig. 9b). The distribution of pore sizes and the pore shape in H2 type is not well defined or irregular [65, 66]. Moreover, the type H2 loop is believed to be associated with ink bottle-like pores of varying radius [67]. The BET analysis showed that the porous sample structure of the thermal dehydration I is the characteristic of pore size distribution in the range of 2 nm to 100 nm, which could be due to the strong porous structure of the thermal dehydration I sample (the inset in Fig. 9b).

The Arshad and Maaroufi method

To find the most probable reaction mechanism using the Arshad and Maaroufi method, Eq. (7) is used. The $h(\alpha)$ curves for the thermoanalytical data of the thermal

dehydrations (I and II) of $Cu_4SO_4(OH)_6$ at $\beta = 10$ °C min^{-1} are presented in Fig. 7a, b, respectively. As shown, the $h(\alpha)$ curves form for the thermal dehydrations I and II follows the A_m- and the D_n-type equations [Deceleratory rate equations (based on the diffusion mechanism)], respectively. Hence, the results of the Arshad and Maaroufi method are not valid for the thermal dehydrations (I and II) of $Cu_4SO_4(OH)_6$.

The iterative procedure

To find the most probable reaction mechanism using the iterative procedure, Eq. (8) is used. The degrees of conversion for $\beta = 5$, 10, 15, and 20 °C min^{-1} at the same temperature for the thermal dehydrations (I and II) of $Cu_4SO_4(OH)_6$ are listed in Table 5. The appropriate temperatures are randomly selected, and the range of α corresponding to the temperature should be within 0.1–0.9. The corresponding degrees of conversion of three temperatures are chosen as examples to put into 35 types of mechanism functions (Table 1).

The slope, correlation coefficient, i.e., r, and intercept of linear regression of $\ln(g(\alpha))$ versus $\ln(\beta)$ are obtained. The results of the linear regression for the thermal dehydration I of $Cu_4SO_4(OH)_6$ show that the slopes of A_2 ($g(\alpha) = [-\ln(1-\alpha)]^{1/2}$) mechanism function are the most adjacent to 1, and the correlation coefficients are better, which are listed in Table 6. Therefore, A_2, which belongs to the mechanism of interface controlled [62]), is determined to be the most probable mechanism function of the thermal dehydration I of $Cu_4SO_4(OH)_6$.

Also, the results of the linear regression for the thermal dehydration II of $Cu_4SO_4(OH)_6$ show that the slopes of A_3 ($g(\alpha) = [-\ln(1-\alpha)]^{1/3}$) mechanism function are the most adjacent to 1, and the correlation coefficients are better, which are listed in Table 6. Therefore, A_3, which belongs to the mechanism of interface controlled [62]), is determined to be the most probable mechanism function of the thermal dehydration II of $Cu_4SO_4(OH)_6$. Therefore, according to the iterative procedure, mechanism of the thermal dehydrations I and II of $Cu_4SO_4(OH)_6$ is the interface controlled. Hence, even though the obtained model types

Table 6 Relation between temperature and degrees of conversion (α) at different heating rates β (°C min^{-1}) and results of $\ln[g(\alpha)]$ versus $\ln(\beta)$ curves of four types of probable mechanism functions for the thermal dehydration of precursor $Cu_4SO_4(OH)_6$

Reaction	T/°C	α				Reaction function	Slope	r
		$\beta = 5$/°C min^{-1}	$\beta = 10$/°C min^{-1}	$\beta = 15$/°C min^{-1}	$\beta = 20$/°C min^{-1}			
Dehydration I	110	0.830	0.638	0.281	0.079	F_2	−2.816	0.959
						F_3	−3.708	0.978
						A_2	−1.046	0.929
						A_3	−0.697	0.929
	112	0.859	0.678	0.316	0.101	F_2	−2.808	0.965
						F_3	−3.813	0.982
						A_2	−1.001	0.933
						A_3	−0.667	0.933
	114	0.886	0.717	0.353	0.124	F_2	−2.825	0.969
						F_3	−3.958	0.985
						A_2	−0.963	0.937
						A_3	−0.642	0.937
Dehydration II	236	0.995	0.880	0.352	0.031	F_2	−6.094	0.987
						F_3	−9.512	0.999
						A_2	−1.707	0.913
						A_3	−1.138	0.913
	237	0.996	0.901	0.389	0.039	F_2	−6.168	0.989
						F_3	−9.835	0.999
						A_2	−1.643	0.916
						A_3	−1.096	0.917
	238	0.998	0.919	0.427	0.051	F_2	−6.380	0.993
						F_3	−10.423	1.000
						A_2	−1.594	0.920
						A_3	−1.063	0.919

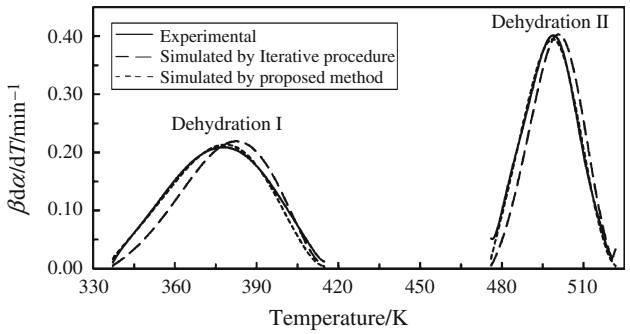

Fig. 10 Comparison of experimental reaction rate and that predicated from the proposed method (Eq. 16) and the iterative procedure (Eq. 8) versus temperature for the thermal dehydrations I and II of precursor $Cu_4SO_4(OH)_6$ at the heating rate of 10 °C min^{-1} in argon

by the proposed method and the iterative procedure are the Avrami–Erofeev, the obtained mechanism results by the iterative procedure are not proved using HRSEM and BET. The reaction model parameters for the iterative procedure are given in Table 5.

Calculation of pre-exponential factor (A_α)

If the reaction follows single-step kinetics and its reaction model is known, Eq. (2) can be rearranged as follows:

$$\ln\left(\frac{d\alpha}{dt}\exp\left(\frac{E_\alpha}{RT}\right)\right) = \ln(A_\alpha) + \ln(f(\alpha)) \tag{24}$$

Equation (24) is the equation of straight line with E_α as the activation energy for the single-step reaction. The value of pre-exponential factor can be calculated by the intercept of the straight line. On the other hand, if the reaction follows multi-step kinetics, pre-exponential factor(s) at each value of "α" can be calculated by Eq. (25) as:

$$\ln\left(\frac{d\alpha}{dt}\right) = -\frac{E_\alpha}{RT_\alpha} + \ln(A_\alpha f(\alpha)) = -\frac{E_\alpha}{RT_\alpha} + C_\alpha \tag{25}$$

where C_α is the intercept of the straight line of $\ln(d\alpha/dt)$ versus $1/T_\alpha$. If reaction model(s) in the multi-step kinetics is/are known over the whole domain of α, then the following equation is helpful to determine the pre-exponential factor(s) over that domain:

$$C_\alpha = \ln(A_\alpha f(\alpha)) \rightarrow A_\alpha = \frac{\exp(C_\alpha)}{f(\alpha)} \tag{26}$$

The pre-exponential factors for the proposed method and the iterative procedure are given in Table 5. Accordingly, the comparison of theoretically fitted reaction rates of the thermal dehydrations (I and II) of $Cu_4SO_4(OH)_6$ under the two methodologies in Fig. 10 (β = 10 °C min^{-1}) emphasizes that the proposed methodology seems more efficient than the iterative procedure (and other well-known methods). It can be mentioned that the proposed method provides basis for the detection of a number of new reaction models capable of dealing with complex processes which could be more complicated mathematically.

Furthermore, it should be mentioned that the kinetics results of the proposed method and iterative procedure presented in the paper were obtained using the programs compiled by ourselves with MATLAB.

Conclusions

The results showed that it is a major limitation that the well-known reaction model determination methods are according to either the choice of constant Arrhenius parameters (apparent activation energy, apparent pre-exponential factor), the use of approximations or the focus on the kinetic compensation principle. To solve this problem, an advanced method for the determination of reaction mechanism model based on the Arrhenius parameter variations was proposed.

This method appears to accurately simulate single-step as well as multi-step reactions kinetics. The proposed method was experimentally verified by taking an experimental example of non-isothermal decomposition kinetics of $Cu_4SO_4(OH)_6$ for the tenorite (CuO) nanoparticles preparation. The results showed that

1. Based on the Vyazovkin method, E_α showed an almost stable behavior with the average of $E_\alpha = 32.3 \pm 2.1$ and 63.9 ± 1.1 kJ mol^{-1} for thermal dehydration I and dehydration II, respectively.
2. Based on the proposed method, the mechanism function form follows the Avrami–Erofeev A_m-type equation, $m(1-\alpha)[-\ln(1-\alpha)](1-1/m)$, i.e., $m = 1.453$ (which belongs to diffusion controlled) and $m = 1.908$ (which belongs to interface controlled) for thermal dehydrations I and II, respectively. Moreover, these results were confirmed by the HRSEM (Fig. 8) and BET (Fig. 9).
3. According to the Arshad and Maaroufi method, the $h(\alpha)$ curves form for the thermal dehydrations I and II followed the A_m- and the D_n-type equation [Decelerator rate equations (based on the diffusion mechanism)], respectively. Hence, the results of the Arshad and Maaroufi method are not valid for the thermal dehydrations (I and II) of $Cu_4SO_4(OH)_6$.
4. The comparison of theoretically fitted reaction rates of the thermal dehydrations (I and II) of $Cu_4SO_4(OH)_6$ under the two methodologies, i.e., the iterative procedure and the proposed method, showed the proposed methodology seems more efficient than the iterative procedure.

5. The proposed methodology seems to be more efficient than the Arshad and Maaroufi method and the iterative procedure as well as other well-known methods. Moreover, the proposed method provides basis for the detection of a number of new reaction models capable of dealing with complex processes which could be more complicated mathematically.

References

1. Tomashevitch KV, Kalinin SV, Vertegel AA, Oleinikov NN, Ketsko VA, Tretyakov YD. Application of non-linear heating regime for the determination of activation energy and kinetic parameters of solid-state reactions. Thermochim Acta. 1998;323:101–7.
2. Arshad MA, Maaroufi AK. An innovative reaction model determination methodology in solid state kinetics based on variable activation energy. Thermochim Acta. 2014;585:25–35.
3. Carr RW. Modeling of chemical reactions. 1st ed. Amsterdam: Elsevier Science; 2007.
4. Wan J, Bu ZY, Xu CJ, Li BG, Fan H. Preparation, curing kinetics, and properties of a novel low-volatile starlike aliphatic-polyamine curing agent for epoxy resins. Chem Eng J. 2011;171:357–67.
5. Santiago D, Francos XF, Ramis X, Salla JM, Sangermano M. Comparative curing kinetics and thermal–mechanical properties of DGEBA thermosets cured with a hyperbranched poly (ethyleneimine) and an aliphatic triamine. Thermochim Acta. 2011;526:9–21.
6. Koga N, Criado JM, Tanaka H. Reaction pathway and kinetics of the thermal decomposition of synthetic brochantite. J Therm Anal. 1997;49:1467–75.
7. Schlesinger ME, King MJ, Sole KC, Davenport WG. Extractive metallurgy of copper. 5th ed. Amsterdam: Elsevier; 2011.
8. Kislik VS. Solvent extraction: classical and novel approaches. 1st ed. Amsterdam: Elsevier; 2012.
9. Greenawalt WE. Hydrometallurgy of copper. 1st ed. West Stockbridge, MA: Hard-Press; 2012.
10. Habashi F. A textbook of hydrometallurgy. 1st ed. Quebec: Metallurgie Extractive; 1993.
11. Gupta CK, Mukherjee TK. Hydrometallurgy in extraction processes. 1st ed. Boca Raton, FL: CRC Press; 1990.
12. Bakhtiari F, Darezereshki E. Synthesis and characterization of tenorite (CuO) nanoparticles from smelting furnace dust (SFD). J Min Metall Sect B Metall. 2013;49:21–6.
13. Darezereshki E, Bakhtiari F. A novel technique to synthesis of tenorite (CuO) nanoparticles from low concentration $CuSO_4$ solution. J Min Metall Sect B Metall. 2011;47:73–8.
14. Darezereshki E, Alizadeh M, Bakhtiari F, Schaffie M, Ranjbar M. A novel thermal decomposition method for the synthesis of ZnO nanoparticles from low concentration $ZnSO_4$ solutions. Appl Clay Sci. 2011;54:107–11.
15. Mirghiasi Z, Bakhtiari F, Darezereshki E, Esmaeilzadeh E. Preparation and characterization of CaO nanoparticles from $Ca(OH)_2$ by direct thermal decomposition method. J Ind Eng Chem. 2014;20:113–7.
16. Dalvand H, Khayati GR, Esmaeilzadeh E, Irannejad A. A facile fabrication of NiO nanoparticles from spent Ni–Cd batteries. Mater Lett. 2014;130:54–6.
17. Vyazovkin S, Burnham AK, Criado JM, Perez-Maqueda LA, Popescu C, Sbirrazzuoli N. ICTAC Kinetics Committee recommendations for performing kinetic computations on thermal analysis data. Thermochim Acta. 2011;520:1–19.
18. Liu XW, Feng YL, Li HR, Zhang P, Wang P. Thermal decomposition kinetics of magnesite from thermogravimetric data. J Therm Anal Calorim. 2011;107:407–12.
19. Verma UN, Mukhopadhyay K. Solid state kinetics of Cu (II) complex of [2-(1,2,3,4-thiatriazole-5-yliminomethyl)-phenol] from thermo gravimetric analysis. J Therm Anal Calorim. 2011;104:1071–5.
20. Selvakumar J, Raghunathan VS, Nagaraja KS. Sublimation kinetics of scandium β-diketonates. J Therm Anal Calorim. 2010;100:155–61.
21. Shahcheraghi SH, Khayati GR. Arrhenius parameters determination in non-isothermal conditions for mechanically activated Ag_2O–graphite mixture. J Trans Nonferrous Met Soc China. 2014;24:3994–4003.
22. Shahcheraghi SH, Khayati GR. Kinetics analysis of the non-isothermal decomposition of Ag_2O–graphite mixture. J Trans Nonferrous Met Soc China. 2014;24:2991–3000.
23. Shahcheraghi SH, Khayati GR. The effect of mechanical activation on non-isothermal decomposition kinetics of Ag_2O–graphite mixture. Arab J Sci Eng. 2014;39:7503–12.
24. Vyazovkin S. Model-free kinetics: staying free of multiplying entities without necessity. J Therm Anal Calorim. 2006;83:45–51.
25. Chrissafis K. Complementary use of isoconversional and model-fitting methods. J Therm Anal Calorim. 2009;95:273–83.
26. Vyazovkin S, Wight CA. Model-free and model-fitting approaches to kinetic analysis of isothermal and non-isothermal data. Thermochim Acta. 1999;340–341:53–68.
27. Vyazovkin S. Thermal analysis. Anal Chem. 2010;82:4936–49.
28. Sbirrazzuoli N. Is the Friedman method applicable to transformations with temperature dependent reaction heat? Macromol Chem Phys. 2007;208:1592–7.
29. Vyazovkin S, Sbirrazzuoli N. Kinetic analysis of isothermal cures performed below the limiting glass transition temperature. Macromol Rapid Commun. 2000;21:85–90.
30. Vyazovkin S. Modification of the integral isoconversional method to account for variation in the activation energy. J Comput Chem. 2001;22:178–83.
31. Gao Z, Amasaki I, Nakada M. A description of kinetics of thermal decomposition of calcium oxalate monohydrate by means of the accommodated R_n model. Thermochim Acta. 2002;385:95–103.
32. Guan CX, Shen YF, Chen DH. Comparative method to evaluate reliable kinetic triplets of thermal decomposition reactions. J Therm Anal Calorim. 2004;76:203–16.
33. Li LQ, Chen DH. Application of iso-temperature method of multiple rate to kinetic analysis: dehydration for calcium oxalate monohydrate. J Therm Anal Calorim. 2004;78:283–93.
34. Genieva SD, Vlaev LT, Atanassov AN. Study of the thermo-oxidative degradation kinetics of poly (tetrafluoroethene) using iso-conversional calculation procedure. J Therm Anal Calorim. 2010;99:551–61.
35. Chen Z, Chai Q, Liao S, Chen X, He Y, Li Y, Wu W, Li B. Non-isothermal Kinetic Study: IV. Comparative methods to evaluate E_a for thermal decomposition of $KZn_2(PO_4)(HPO_4)$ synthesized by a simple route. Ind Eng Chem Res. 2012;51:8985–91.
36. Miura K, Maki T. A simple method for estimating $f(E)$ and $k_0(E)$ in the distributed activation energy model. Energy Fuels. 1998;12:864–9.
37. Burnham AK, Braun RL. Global kinetic analysis of complex materials. Energy Fuels. 1999;13:1–22.
38. Cai J, He F, Yao F. Non-isothermal nth-order DAEM equation and its parametric study: use in the kinetic analysis of biomass pyrolysis. J Math Chem. 2007;42:949–56.
39. Boonchom B. Kinetic and thermodynamic studies of $MgHPO_4$-$3H_2O$ by non-isothermal decomposition data. J Therm Anal Calorim. 2009;98:863–71.

40. Langford JI, Wilson AJC. Scherrer after sixty years: a survey and some new results in the determination of crystallite size. J Appl Cryst. 1978;11:102–13.
41. Bakhtiari F, Darezereshki E. One-step synthesis of tenorite (CuO) nano-particles from Cu_4 (SO_4) $(OH)_6$ by direct thermal-decomposition method. Matter Lett. 2011;65:171–4.
42. Suryanarayana C. Mechanical alloying and milling. Prog Mater Sci. 2001;46:1–184.
43. Secco EA. Spectroscopic properties of SO_4 (and OH) in different molecular and crystalline environments. I. Infrared spectra of $Cu_4(OH)_6SO_4$, $Cu_4(OH)_4OSO_4$, and $Cu_3(OH)_4SO_4$. Can J Chem. 1988;66:329–36.
44. Stoch A, Stoch J, Gurbiel J, Cichocinska M, Mikolajczyk M, Timler M. FTIR study of copper patinas in the urban atmosphere. J Mol Struct. 2001;596:201–6.
45. Guedes M, Ferreira JM, Ferro AC. A study on the aqueous dispersion mechanism of CuO powders using Tiron. J Colloid Interface Sci. 2009;330:119–24.
46. Chen L, Li L, Li G. Synthesis of CuO nanorods and their catalytic activity in the thermal decomposition of ammonium perchlorate. J Alloys Compd. 2008;464:532–6.
47. Fernandes DM, Silva R, Hechenleitner AAW, Radovanovic E, Melo MAC, Pineda EAG. Synthesis and characterization of ZnO, CuO and a mixed Zn and Cu oxide. Mater Chem Phys. 2009;115:110–5.
48. Darezereshki E. Synthesis of maghemite (γ-Fe_2O_3) nanoparticles by wet chemical method at room temperature. Mater Lett. 2010;64:1471–2.
49. Cao G. Nanostructures and nanomaterials: synthesis, properties and applications. 1st ed. London: Imperial College Press; 2004.
50. Castro R, Benthem KV. Sintering: mechanisms of convention nanodensification and field assisted processes. 1st ed. Berlin: Springer; 2012.
51. Lu K. Nanoparticulate materials: synthesis, characterization, and processing. 1st ed. New York: Wiley-VCH Inc; 2012.
52. Hosokawa M, Nogi K, Naito M, Yokoyama T. Nanoparticle technology handbook. 2nd ed. Amsterdam: Elsevier; 2012.
53. Khayati GR, Janghorban K. An investigation on the application of process control agents in the preparation and consolidation behavior of nanocrystalline silver by mechanochemical method. Adv Powder Technol. 2012;23:808–13.
54. Khayati GR, Janghorban K. Thermodynamic approach to synthesis of silver nanocrystalline by mechanical milling silver oxide. J Trans Nonferrous Met Soc China. 2013;23:543–7.
55. Khayati GR, Dalvand H, Darezereshki E, Irannejad A. A facile method to synthesis of CdO nanoparticles from spent Ni–Cd batteries. Matter Lett. 2014;115:272–4.
56. Habashi F. Recent trends in extractive metallurgy. J Min Metall Sect B Metall. 2009;45:1–13.
57. Gaskell DR. Introduction to metallurgical thermodynamics. 4th ed. London: Taylor & Francis Books Inc; 2003.
58. Jankovic B, Mentus S, Jelic D. A kinetic study of non-isothermal decomposition process of anhydrous nickel nitrate under air atmosphere. Phys B. 2009;404:2263–9.
59. Boonchom B. Kinetics and thermodynamic properties of the thermal decomposition of manganese di hydrogen phosphate dehydrate. J Chem Eng Data. 2008;53:1533–8.
60. Gao X, Dollimore D. The thermal decomposition of oxalates: Part 26. A kinetic study of the thermal decomposition of manganese (II) oxalate dehydrate. Thermochim Acta. 1993;215:47–63.
61. Vlaev LT, Nikolova MM, Gospodinov GG. Non-isothermal kinetics of dehydration of some selenite hexahydrates. J Solid State Chem. 2004;177:2663–9.
62. Jackson KA. Kinetic processes: crystal growth, diffusion, and phase transitions in materials. 1st ed. New York: Wiley-VCH Inc; 2010.
63. Brunauer S, Emmett PH, Teller E. Adsorption of gases in multimolecular layers. J Am Chem Soc. 1938;60:309–19.
64. Brunauer S, Deming LS, Deming WE, Teller E. On a theory of the van der Waals adsorption of gases. J Am Chem Soc. 1938;62:1723–32.
65. Sing KSW, Everett DH, Haul RAW, Moscou L, Pierotti RA, Rouquerol J, Siemieniewska T. Reporting physisorption data for gas/solid systems with special reference to the determination of surface area and porosity. Pure Appl Chem. 1982;54:2201–18.
66. Ertl G, Knozinger H, Schuth F, Weitkamp J. Handbook of heterogeneous catalysis. 1st ed. Weinheim: Wiley-VCH Verlag GmbH & Co., KGaA; 2008.
67. Gregg SJ, Sing KSW. Adsorption, surface area and porosity. 1st ed. London: Academic Press; 1974.